

DOI: 10.1002/cbic.200700003

A Two-Photon Fluorescent Probe for Lipid Raft Imaging: C-Laurdan

Hwan Myung Kim,^[a] Hyo-Jung Choo,^[b] Soon-Young Jung,^[b] Young-Gyu Ko,^{*[b]}
 Won-Hwa Park,^[a] Seung-Joon Jeon,^{*[a]} Chul Hoon Kim,^[c] Taiha Joo,^{*[c]} and
 Bong Rae Cho^{*[a]}

The lipid-rafts hypothesis proposes that naturally occurring lipid aggregates exist in the plane of membrane that are involved in signal transduction, protein sorting, and membrane transport. To understand their roles in cell biology, a direct visualization of such domains in living cells is essential. For this purpose, 6-dodecanoyl-2-(dimethylamino)naphthalene (laurdan), a membrane probe that is sensitive to the polarity of the membrane, has often been used. We have synthesized and characterized 6-dodecanoyl-

2-[N-methyl-N-(carboxymethyl)amino]naphthalene (C-laurdan), which has the advantages of greater sensitivity to the membrane polarity, a brighter two-photon fluorescence image, and reflecting the cell environment more accurately than laurdan. Lipid rafts can be visualized by two-photon microscopy by using C-laurdan as a probe. Our results show that the lipid rafts cover 38% of the cell surface.

Introduction

Among the fluid phospholipids in the plasma membrane are rigid compartments composed of glycosphingolipids and cholesterol. These compartments accommodate many cellular molecules that mediate different cellular procedures such as signal transduction, pathogen invasion, cholesterol homeostasis, neurodegenerative diseases, and angiogenesis.^[1–5] The existence of submicrometer-sized compartments, also called lipid rafts, has been demonstrated in mammalian cells and in model membranes by using various techniques such as atomic-force microscopy, fluorescence microscopy, and coherent anti-Stokes Raman scattering microscopy.^[6–12] To understand their roles in cell biology, a direct visualization of such domains in living cells is essential. Recently, it was reported that lipid rafts in living cells can be visualized by generalized polarization (GP) images of cells that have been labeled with 6-dodecanoyl-2-(dimethylamino)naphthalene (laurdan) by using two-photon microscopy (TPM).^[13] However, neither the center GP value nor the coverage of the high GP domain changed appreciably upon treatment with methyl β -cyclodextrin (M β CD), a lipid-raft-destroying reagent. This indicates that laurdan does not accurately reflect the fluid and gel domains in the plasma membrane. Moreover, the literature results based on laurdan are difficult to reproduce. Therefore, there is a pressing need to develop a more efficient two-photon probe for lipid raft imaging.


To design an efficient two-photon probe for the lipid rafts, we considered several requirements: 1) a significant two-photon cross section in the 700–1000 nm range, which is necessary to obtain a clear TPM image at low dye concentration; 2) appreciable water solubility for staining; 3) a high sensitivity to the membrane polarity; 4) the capability to stain the fluid and gel domains in the plasma membrane without producing

aggregates. Because laurdan behaves ideally in giant unilamellar vesicles (GUVs) composed of 1,2-dipalmitoyl-*sn*-glycero-3-phosphocholine (DPPC),^[14] but not in cells, we thought that the negligible solubility of laurdan in water might be responsible for the problems. Therefore, we have introduced a carboxylic acid moiety to laurdan to improve its water solubility while keeping the other functional groups intact. Herein, we report that 6-dodecanoyl-2-[N-methyl-N-(carboxymethyl)amino]naphthalene (C-laurdan) is an efficient two-photon (TP) probe that meets all of the requirements as outlined above. Furthermore, the existence of the lipid rafts in mammalian cells has been unambiguously established by using C-laurdan as a TP polarity probe.

[a] H. M. Kim, W.-H. Park, Prof. Dr. S.-J. Jeon, Prof. Dr. B. R. Cho
 Department of Chemistry and
 Center for Electro- and Photo-Responsive Molecules, Korea University
 1-Anamdong, Seoul, 136-701 (Korea)
 Fax: (+82)2-3290-3544
 E-mail: chobr@korea.ac.kr

[b] H.-J. Choo, S.-Y. Jung, Prof. Dr. Y.-G. Ko
 Graduate School of Life Sciences and Biotechnology, Korea University
 1-Anamdong, Seoul, 136-701 (Korea)

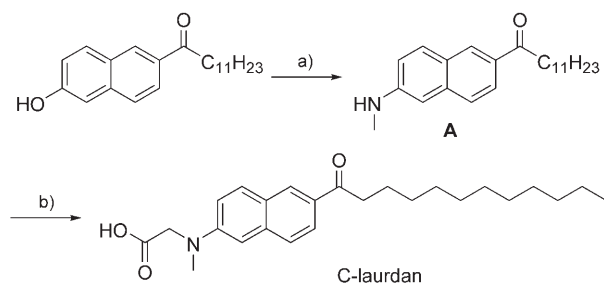
[c] C. H. Kim, Prof. Dr. T. Joo
 Department of Chemistry, Pohang University of Science and Technology
 Pohang 790784 (Korea)

 Supporting information for this article is available on the WWW under <http://www.chembiochem.org> or from the author.

Results and Discussion

Synthesis of C-laurdan

C-laurdan was synthesized in good yield from the reaction between 6-dodecanoyl-*N*-methyl-2-naphthylamine (**A**) and methyl bromoacetate, followed by the hydrolysis of the methyl ester (Scheme 1). Amine **A** was prepared by the amination of 2-hydroxy-6-dodecanoylnaphthalene as previously reported.^[15]



Scheme 1. Reagents and conditions: a) $\text{Na}_2\text{S}_2\text{O}_5/\text{CH}_3\text{NH}_2\text{HCl}/\text{NaOH}/\text{H}_2\text{O}$; b) i: $\text{BrCH}_2\text{CO}_2\text{CH}_3/\text{proton-sponge}/\text{MeCN}$, ii: KOH/EtOH .

Spectroscopic properties in solution and model membranes

The water solubility was determined by measuring the fluorescence intensity as a function of the dye concentration. The solubility of C-laurdan in water is $3.0\ \mu\text{M}$, whereas laurdan is virtually insoluble in water and produces aggregates at $0.1\ \mu\text{M}$ (see Figure S3 in the Supporting Information). The higher solubility

of C-laurdan can be ascribed to the carboxylic acid moiety ($\text{p}K_a=6.4$), which can be solvated by water (Supporting Information). This indicates that our design strategy is efficient in providing water solubility.

The fluorescence spectra of laurdan show gradual bathochromic shifts with the solvent polarity in the order $\text{c-Hex} < \text{DMF} < \text{EtOH}$ (Figure 1A). In water however, the spectrum is blue-shifted and the emission is very weak ($\Phi=0.01$; Table 1). In contrast, the fluorescence of C-laurdan shows systematic bathochromic shifts in all of the solvents employed in this study (Figure 1b). This indicates that C-laurdan has a higher sensitivity to the solvent polarity than laurdan.

A similar result was observed in the vesicles (Figure 1C and D). In DPPC, laurdan shows $\lambda_{\text{fl}}^{\text{max}}$ at 440 nm, whereas in 1,2-dioleoyl-*sn*-glycero-3-phosphocholine (DOPC) it shows a broad spectrum that can be dissected into two bands centered at 439 and 484 nm (Figure 1C). The emission spectra of laurdan in DOPC/sphingomyelin/cholesterol (1:1:1, raft mixture) and DPPC show reasonable overlap, which indicates that this probe preferentially reflects the gel domain compared to the fluid domain in the raft mixture. In contrast, C-laurdan shows discrete $\lambda_{\text{fl}}^{\text{max}}$ at 442 and 486 nm in DPPC and DOPC, respectively (Figure 1D). Moreover, the emission spectrum of the C-laurdan in the raft mixture is broad, and is almost the same as the sum of the spectra in DPPC and DOPC; that is, C-laurdan accurately reflects the rigid and fluid domains in the vesicles.

Time-resolved fluorescence (TRF) spectra provided a clue as to the spectral difference between the two probes in solution (Figure S5). In ethanol, in which both are readily soluble, the TRFs show ultrafast intramolecular charge transfer (ICT) fol-

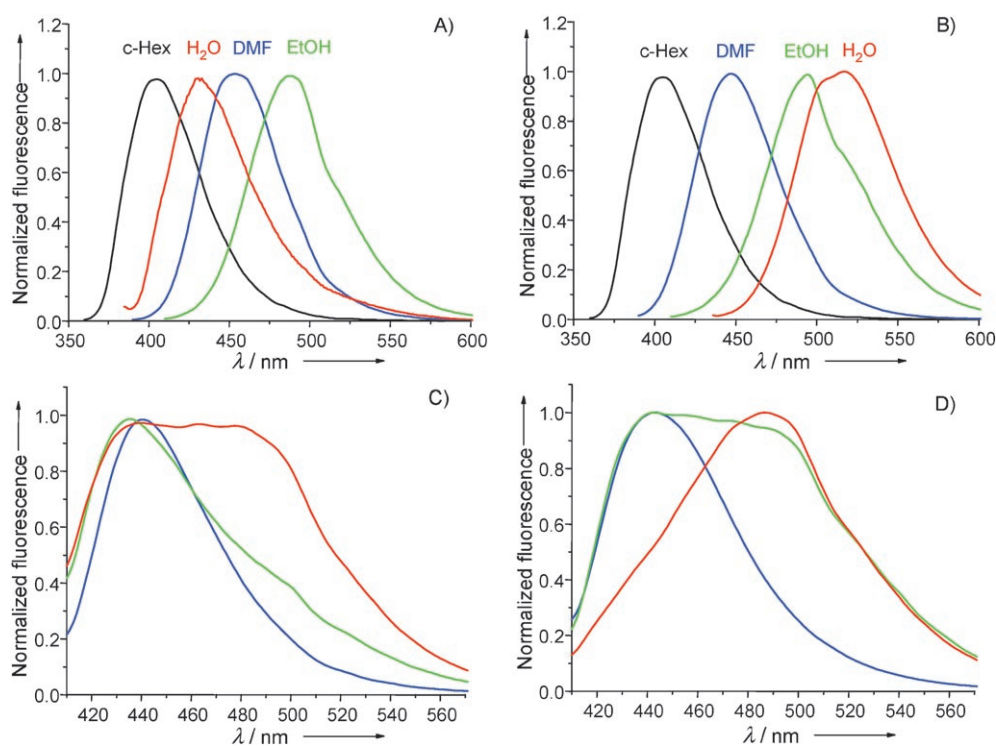


Figure 1. Normalized emission spectra of A) laurdan and B) C-laurdan in cyclohexane, DMF, EtOH, and H_2O . Normalized emission spectra of C) laurdan and D) C-laurdan in the phospholipid vesicles composed of DPPC (blue), DOPC (red), and DOPC/sphingomyelin/cholesterol (1:1:1; green) at $24.7\ ^\circ\text{C}$.

Solvent	$\lambda_{\text{max}}^{(a)}$		$\lambda_{\text{fl}}^{\text{max}(b)}$		$\lambda_{\text{max}}^{(c)}$		$\phi^{(d)}$		$\delta_{\text{max}}^{(e)}$	
	L	CL	L	CL	L	CL	L	CL	L	CL
c-Hex	344	345	407	404	ND	ND	0.11	0.10	ND	ND
DMF	356	363	454	446	780	780	1.0	0.36	50	170
EtOH	363	383	487	494	780	780	1.0	0.43	60	150
H ₂ O	354	384	431	522	ND	820	0.01	0.11	ND	320

[a,b] λ_{max} of the one-photon absorption and emission spectra in nm. [c] λ_{max} of the two-photon excitation spectra in nm. [d] Fluorescence quantum yield. [e] The peak two-photon absorptivity in $10^{-50} \text{ cm}^4 \text{ s}$ per photon (GM). The experimental uncertainty is of the order of 10–15%.

lowed by solvation; this indicates that both compounds emit from the ICT states. In water, the TRF of C-laurdan indicates ICT/solvation, while that of laurdan reveals the existence of aggregate and provides no evidence for relaxation (Figure S5, Table S1). Therefore, C-laurdan emits from the ICT state in both solvents, and shows a gradual bathochromic shift with the solvent polarity, whereas laurdan emits from the locally excited (LE) state in water to result in a blue-shifted and weak fluorescence. This is because laurdan exists as aggregates due to its negligible water solubility.

In a DPPC and raft mixture, laurdan does not undergo ICT/solvation and emits from the LE state to result in a blue-shifted spectrum (Figure S6). In DOPC, the ICT/solvation is relatively slow (Table S2), and the emission occurs from both the LE and ICT states to give rise to a broad spectrum. In contrast, C-laurdan undergoes ICT/solvation in all of the vesicles employed in this study (Table S2). In DPPC however, only a small fraction of C-laurdan undergoes ICT/solvation, and emission occurs mostly from the LE state. In DOPC, most of the C-laurdan molecules undergo fast ICT/solvation to give emission mostly in the red. In the raft mixture, the TRF signals show behavior that is roughly the average of those found in DPPC and DOPC, and the emission occurs from both the LE and ICT states to result in a broad spectrum. Thus TRFs establish that C-laurdan reflects the dipolar nature of the vesicle environments much more accurately than laurdan.

The two-photon cross sections (δ_{TPA}) of laurdan and C-laurdan were measured by using 200 fs pulses (Figure S7).^[16–18] The values of δ_{max} for the two probes in EtOH are 60 and 150 GM (1 GM = $10^{-50} \text{ cm}^4 \text{ s}$ per photon) at 780 nm, respectively. In water, the δ_{max} value of C-laurdan was 320 GM at 820 nm, whereas that of laurdan could not be measured because the

two-photon excited fluorescence (TPEF) was too weak to detect (Table 1).

Two-photon excitation with polarized light provided detailed information about the alignment of the probes in the bilayer.^[19] The GUVs composed of DPPC revealed a weak fluorescent area perpendicular to the excitation polarization, regardless of which probes were used (Figure 2B and E). A similar result was observed for the raft mixture GUVs (Figure S8). On the other hand, the laurdan-stained DOPC GUVs emitted intense TPEF throughout the equatorial sections of GUVs; this indicates that laurdan is randomly oriented in the GUVs (Figure 2A). In contrast, the C-laurdan-labeled GUVs revealed a

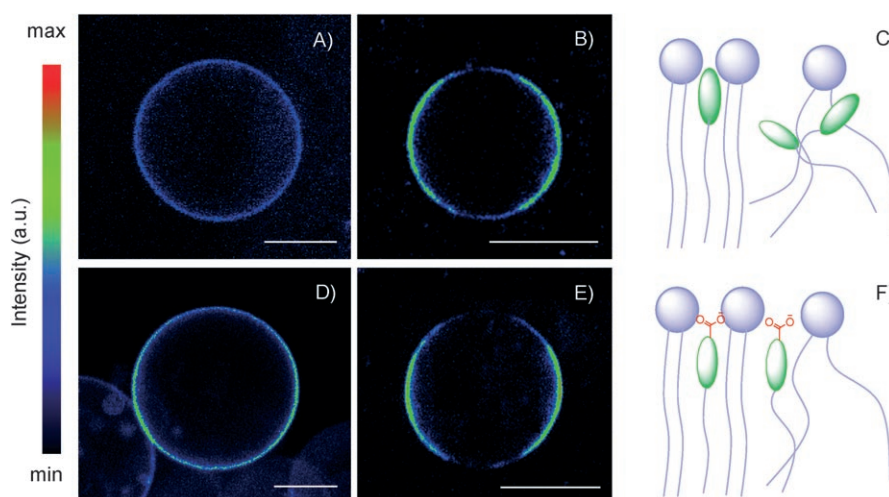


Figure 2. Two-photon fluorescence images of GUVs composed of DOPC (A, D) and DPPC (B, E) labeled with laurdan (A, B) and C-laurdan (D, E). Scale bars = 30 μm . The excitation light ($\lambda = 780 \text{ nm}$, $I = 200\text{--}300 \text{ mW } \mu\text{m}^{-2}$) was polarized parallel to the horizontal axis of the image. Schematic representation of the location of laurdan (C) and C-laurdan (F) in the GUVs.

weak fluorescent area perpendicular to the excitation polarization (Figure 2D); this shows the photoselection effect.^[19] A sketch of the probe location is presented in Figure 2C and F. In the gel phase, both dyes are aligned parallel to the lipid molecules. In the fluid phase, however, laurdan is randomly oriented, whereas C-laurdan can be aligned parallel to the lipid molecules, probably because of the favorable hydrophilic interactions between the carboxylates and the water molecules near the lipid head groups.

GP images of model membranes

The sensitivity of the probes to the membrane polarity was assessed by the GP images (see the Experimental Section).^[12–14]

In all GUVs, the images were brighter when stained with C-laurdan than with laurdan, presumably because of the larger two-photon cross section, and the stronger excitation bands in the vesicles (Figures S2 and S7). For both probes, the GP distribution curves of DPPC GUVs are narrow, while those for DOPC GUVs are broader (Figure 3). When the distribution curves for the raft mixture GUVs are fitted to two Gaussian functions, the center GP values are 0.09 and 0.36 for laurdan-labeled and -0.14 and 0.18 for C-laurdan-labeled GUVs (Figure 3, Table 2). This could be because laurdan emits from the LE state, and this results in overestimated GP values (vide supra). Also, the

lower GP Gaussian function for the laurdan-labeled GUVs is broader than the higher one (Figure 3). In contrast, the two Gaussian functions for the C-laurdan-labeled GUVs are sharp and well separated from the intersection at ~ 0 (Figure 4); that is, this probe reflects the membrane polarity more accurately.

GP images of cells

The TPM images of the A431 cells are much brighter when stained with C-laurdan than with laurdan, probably because of the larger two-photon cross section (Figure S9). The pseudo-

colored GP images of the laurdan-labeled cells revealed that there is little change in the high GP domain before and after treatment with M β CD (Figure 4A and B). Consistently, the high GP curve that is centered at GP = 0.49 decreased slightly upon treatment with M β CD, without appreciable change in the low GP curve at 0.26 (Figure 4C and D). In an ideal situation, the low GP curve should be unaltered while the higher one should disappear upon treatment with M β CD, in order to reflect the existence of rigid lipid raft domain. On the other hand, the high GP domain of the C-laurdan-stained cells disappeared almost completely upon treatment with M β CD; this indicates that there may indeed be lipid rafts (Figure 4E and F). Moreover, the high GP curve decreased dramatically, and the low GP curve became predominant after treatment with M β CD (Figure 4G and H). This outcome is very similar to the ideal one mentioned above. Therefore, the effect of M β CD on the two domains is clearly demonstrated by using C-laurdan.

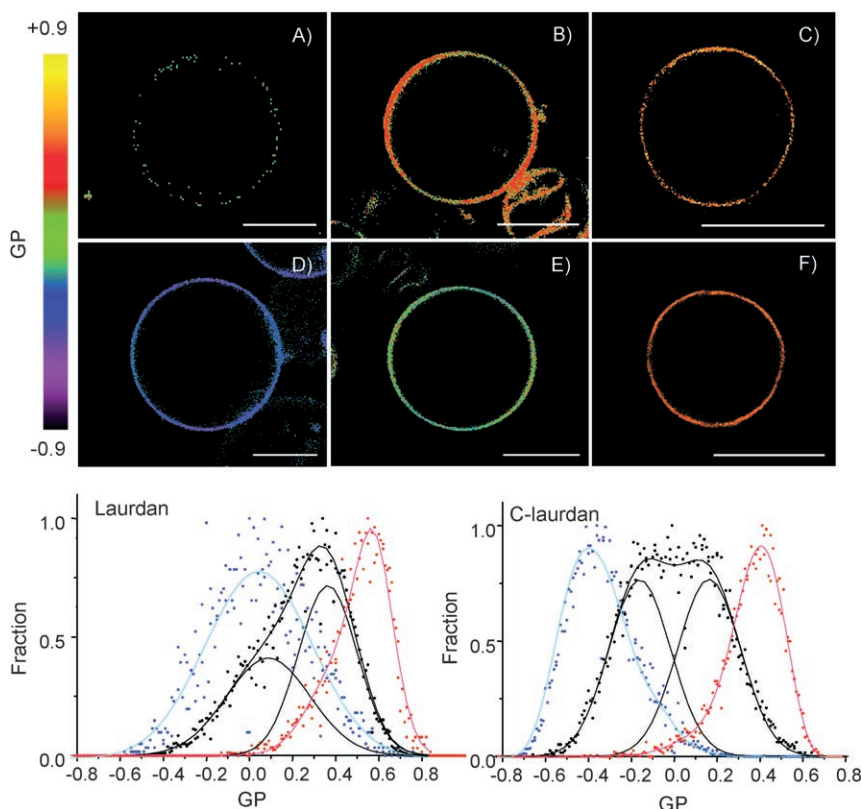


Figure 3. GP images of equatorial section of single GUVs composed of DOPC (A, D), DOPC/sphingomyelin/cholesterol (1:1:1; B, E), and DPPC (C, F) labeled with laurdan (A–C) and C-laurdan (D–F) At 24.7 °C. Excitation wavelength is 780 nm. Scale bars = 30 μ m.

Table 2. Two Gaussian distributions of deconvoluted stacks of GP images.

Sample	Center 1 ^[a]	Width 1 ^[b]	Center 2 ^[c]	Width 2 ^[d]	Coverage 2 [%]
DOPC (laurdan)	0.044 (0.0062) ^[e]	0.50 (0.016) ^[e]			
Raft mixture ^[f] (laurdan)	0.09 (0.054)	0.39 (0.052)	0.36 (0.012)	0.27 (0.015)	
DPPC (laurdan)			0.54 (0.0023) ^[e]	0.25 (0.0049) ^[e]	
DOPC (C-laurdan)	-0.35 (0.0026) ^[e]	0.32 (0.0058) ^[e]			
Raft mixture ^[f] (C-laurdan)	-0.14 (0.012)	0.29 (0.014)	0.18 (0.012)	0.29 (0.014)	
DPPC (C-laurdan)			0.41 (0.0014) ^[e]	0.24 (0.0031) ^[e]	
A431 (laurdan)	0.26 (0.049)	0.42 (0.050)	0.49 (0.0055)	0.22 (0.022)	46
A431 (laurdan-M β CD)	0.22 (0.074)	0.43 (0.070)	0.51 (0.021)	0.28 (0.038)	27
A431 (C-laurdan)	-0.041 (0.011)	0.31 (0.012)	0.28 (0.0098)	0.30 (0.010)	38
A431 (C-laurdan-M β CD)	-0.090 (0.013)	0.41 (0.017)	0.24 (0.022)	0.26 (0.033)	11

[a–d] The center GP values of low and high GP regions and their width in the GP curves fitted to two Gaussian distributions except otherwise noted. The numbers in the parenthesis are the standard deviation. [e] The center GP values and their width in the GP curves fitted to single component. [f] DOPC/sphingomyelin/cholesterol (1:1:1).

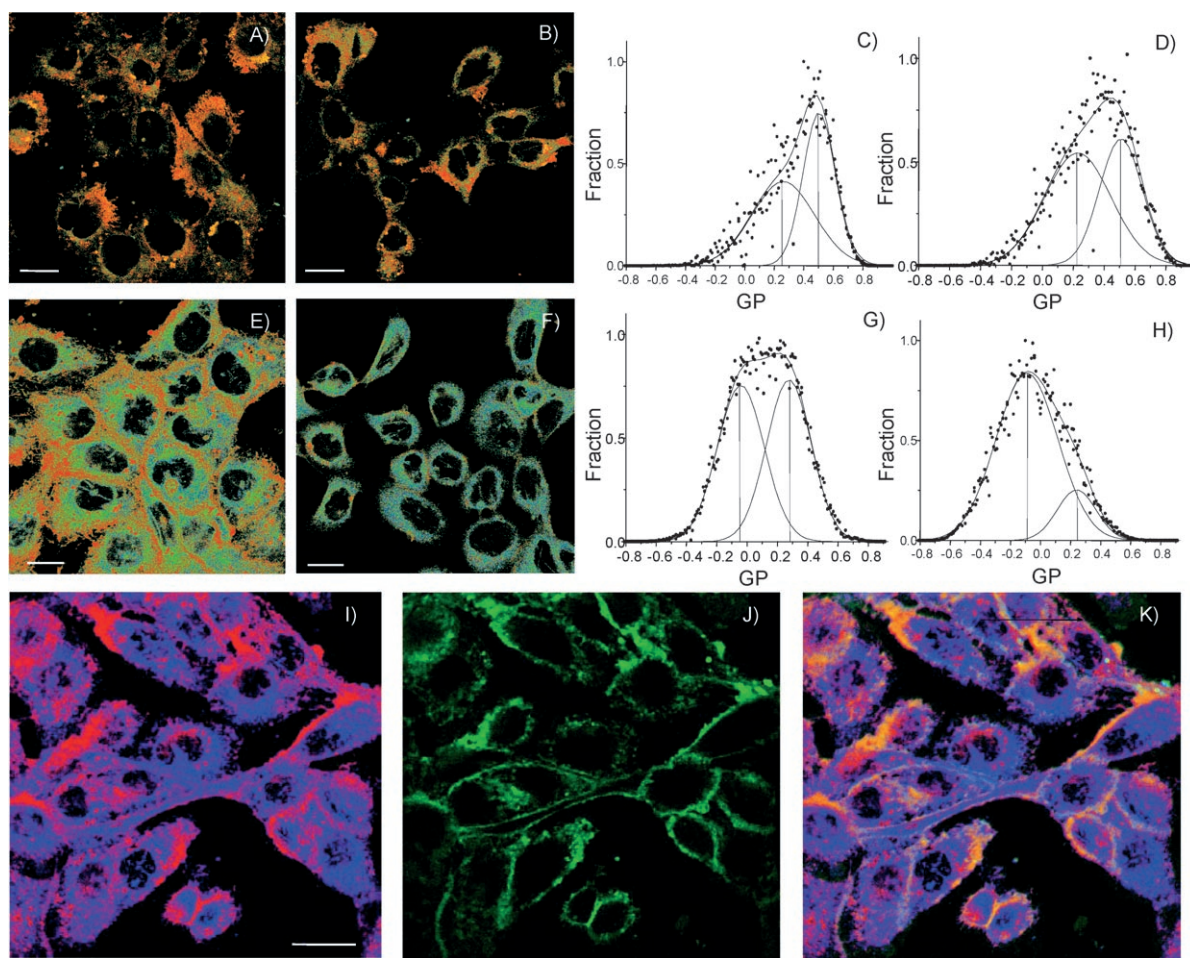


Figure 4. GP images of laurdan-labeled A431 cells A) before and B) after treatment with 10 mM M β CD for 30 min, and GP distribution curves (C, D). GP images of the C-laurdan-labeled A431 cells E) before, and F) after treatment with M β CD and GP distribution curves (G, H). Scale bars = 10 μ m. I) The high GP domains of A431 cells labeled with C-laurdan, J) fluorescence image in the A431 cell labeled with BODIPY-G_{M1} and K) colocalized images. Excitation wavelength is 780 nm. Scale bars = 20 μ m.

The ideal behavior of C-laurdan in cells is due to the ICT/solvation process. The TRFs of the cell-embedded laurdan and C-laurdan showed that C-laurdan undergoes the ICT/solvation process, whereas laurdan does not (Figure 5). That is, only the C-laurdan can accurately reflect the polarity of the environment where it resides, since the sensitivity to the dipolar nature of the environment originates from the ICT/solvation process. Indeed, the TRF of cell-embedded C-laurdan revealed that the ICT/solvation rate increases significantly after treatment with M β CD, which shifts the emission from blue to red (Table S3). In contrast, the TRF of laurdan in A431 cells does not change upon treatment with M β CD, and emits mostly from the LE state to result in overestimated GP values. The GP distribution curves of each section of the cells are depicted in Figures S11 and S12. The GP value increased gradually from the bottom to the top of the cells. The total surface area covered by high GP domains (GP > 0.49) of laurdan-labeled cells is 45%. When the cells were treated with M β CD, this value decreased to 26% (Table 2). On the other hand, the corresponding values for the C-laurdan-labeled cells (GP > 0.28) are 38 and 11%, respectively (Table 2). Here again, C-laurdan is a better indicator for the effect of M β CD.

To unambiguously determine whether the high GP domains in the C-laurdan-labeled cells are indeed due to the lipid rafts, the high GP image was colocalized with the fluorescence image of ganglioside G_{M1}, which is known to be highly enriched in the raft domains,^[20–21] by co-staining A431 cells with C-laurdan and BODIPY-G_{M1} in the plasma membrane. As shown in Figure 4K, the two images overlap almost completely; this confirms that the high GP image reflects lipid rafts. In sharp contrast, the high GP image of the laurdan-labeled cells shows only partial overlap with the fluorescence image of BODIPY-G_{M1} (Figure S10). Hence, the direct visualization of the lipid raft is clearly demonstrated with two-photon microscopy by using C-laurdan as the probe. Furthermore, our results show that the lipid rafts cover 38% of the A431 cell surface, and are enriched on the top edge of the cell.

Because of the strong hydrophilic interactions between the introduced carboxylic acid moiety and water, C-laurdan is more soluble in water, and is located parallel to the cell membrane. Because its emission occurs from both the LE and ICT states, and the amplitude ratio depends upon the polarity of the environment, C-laurdan accurately reflects both the fluid and rigid domains of cells. In contrast, laurdan, which lacks a

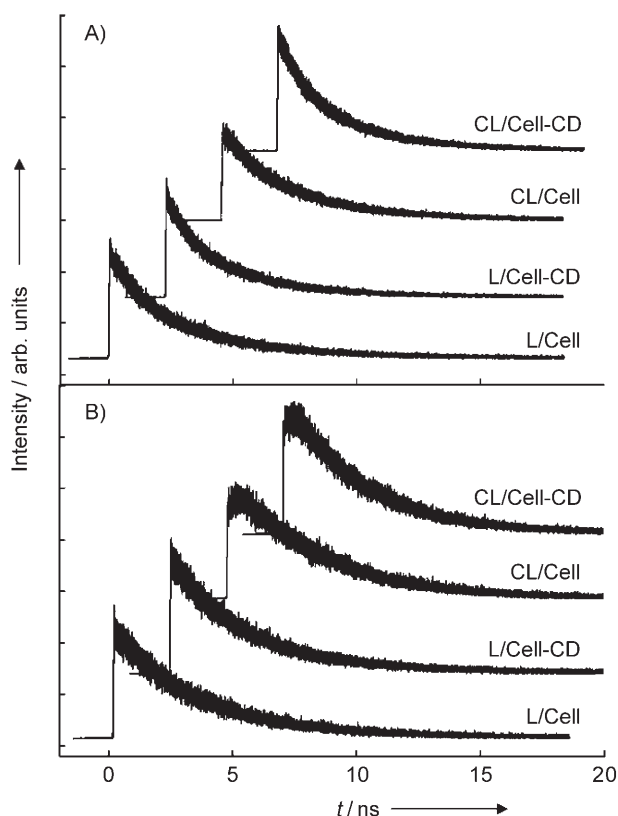


Figure 5. Picosecond time-resolved fluorescence of the laurdan and C-laurdan in A431 cells with and without the treatment with methyl- β -cyclodextrin measured at A) 440 nm and B) 490 nm. Excitation wavelength is 380 nm.

hydrophilic group, cannot be solvated by water molecules, is randomly distributed in the cell membrane, does not undergo ICT/solvation in cells, and emits from the LE state only, which results in overestimated GP curves that do not change much upon treatment with M β CD. Therefore laurdan reflects the cell environment less accurately than C-laurdan.

Conclusions

One of the most important controversies in cell biology is the lipid raft hypothesis.^[22] To directly visualize such domains in the cell, we have developed a new two-photon-fluorescence membrane probe, 6-dodecanoyl-2-[*N*-methyl-*N*-(carboxymethyl)amino]naphthalene (C-laurdan), which has several advantages over laurdan, including a greater sensitivity to the solvent polarity and stronger TPEF emission. Further, it gives a more accurate representation of the cell environment. The stronger TPEF, symmetrical GP distribution curve that can be deconvoluted into two curves with similar shape and area, and the dramatic decrease in the high GP curve upon treatment with M β CD without a concomitant change in the lower one is particularly useful. This compound will find useful applications as an efficient two-photon probe for cell membrane imaging.

Experimental Section

Materials: Synthetic reagents were purchased from Sigma–Aldrich and used without further purification. All solvents were from

Riedel-de Haën (Seelze, Germany) and Sigma–Aldrich and were distilled prior to use. DPPC, DOPC, and sphingomyelin were from Avanti Polar Lipids (Alabaster, AL). Cholesterol was from Sigma–Aldrich. Laurdan was from Molecular Probes (Eugene, OR).

Synthesis of C-laurdan

6-Dodecanoyl-*N*-methyl-2-naphthylamine (A): MeNH₂·HCl (11.0 g, 0.13 mol) was added to a mixture of 2-hydroxy-6-dodecanoylnaphthalene (8.0 g, 25 mmol),^[15] Na₂S₂O₅ (12 g, 61 mmol), NaOH (5.2 g, 0.13 mol), and H₂O (100 mL) in a pressure tube, and the mixture was stirred at 140 °C for 48 h. The product was collected by filtration, washed with water, and purified by crystallization from CH₂Cl₂/EtOH; yield 5.6 g (67%); m.p. 99 °C; ¹H NMR (300 MHz, CDCl₃): δ = 8.31 (s, 1H), 7.94 (dd, *J* = 9.0, 3.0 Hz, 1H), 7.72 (d, *J* = 9.0 Hz, 1H), 7.64 (d, *J* = 9.0 Hz, 1H), 6.91 (dd, *J* = 9.0, 3.0 Hz, 1H), 6.77 (s, 1H), 3.97 (brs, 1H), 3.03 (t, *J* = 7.5 Hz, 2H), 2.97 (s, 3H), 1.77 (quin, *J* = 7.5 Hz, 2H), 1.26 (m, 16H), 0.88 (t, *J* = 7.5 Hz, 3H); ¹³C NMR (75 MHz, CDCl₃): δ = 200.6, 149.3, 138.2, 130.9, 130.9, 130.1, 126.2, 126.2, 125.1, 118.6, 103.3, 38.6, 32.2, 29.9, 29.9, 29.8, 29.8, 29.8, 29.7, 29.6, 25.1, 22.9, 14.4; IR (KBr) $\tilde{\nu}_{\max}$ = 3389, 1663 cm⁻¹; elemental analysis calcd (%) for C₂₃H₃₃NO: C 81.37, H 9.80, N 4.13; found: C 81.31, H 9.88, N 4.09.

C-laurdan: A mixture of A (3.0 g, 8.8 mmol), methyl bromoacetate (2.0 g, 13 mmol), Na₂HPO₄ (1.9 g, 13 mmol), and NaI (0.5 g, 3.5 mmol) in MeCN (50 mL) was refluxed under N₂ for 18 h. The product was extracted with ethyl acetate, washed with brine, and purified by crystallization from EtOH to obtain a light yellow powder; yield 2.5 g (70%); m.p. 68 °C; ¹H NMR (300 MHz, CDCl₃): δ = 8.33 (s, 1H), 7.94 (dd, *J* = 9.0, 3.0 Hz, 1H), 7.82 (d, *J* = 9.0 Hz, 1H), 7.66 (d, *J* = 9.0 Hz, 1H), 7.10 (dd, *J* = 9.0, 3.0 Hz, 1H), 6.88 (s, 1H), 4.23 (s, 2H), 3.74 (s, 3H), 3.21 (s, 3H), 3.04 (t, *J* = 7.5 Hz, 2H), 1.77 (quin, *J* = 7.5 Hz, 2H), 1.26 (m, 16H), 0.88 (t, *J* = 7.5 Hz, 3H); A mixture of this intermediate (2.0 g, 4.9 mmol) and KOH (0.70 g, 12 mmol) in EtOH (50 mL) was stirred for 5 h. The resultant solution was diluted with ice-water (100 mL) and concentrated HCl (aq) was added slowly at <5 °C until pH 3 was reached. The resulting precipitate was collected, washed with distilled water, and purified by crystallization from chloroform/petroleum ether; yield 1.5 g (79%); m.p. 127 °C; ¹H NMR (300 MHz, [D₆]DMSO): δ = 12.70 (brs, 1H), 8.43 (s, 1H), 7.89 (d, *J* = 9.0 Hz, 1H), 7.80 (d, *J* = 9.0 Hz, 1H), 7.66 (d, *J* = 9.0 Hz, 1H), 7.20 (d, *J* = 9.0 Hz, 1H), 6.92 (s, 1H), 4.26 (s, 2H), 3.09 (s, 3H), 3.03 (t, *J* = 7.5 Hz, 2H), 1.61 (quin, *J* = 7.5 Hz, 2H), 1.22 (m, 16H), 0.83 (t, *J* = 7.5 Hz, 3H); ¹³C NMR (75 MHz, [D₆]DMSO): δ = 199.9, 172.4, 149.8, 137.8, 131.3, 130.7, 130.5, 126.7, 125.4, 124.7, 116.7, 105.6, 100.3, 39.8, 38.2, 32.0, 29.7, 29.7, 29.7, 29.7, 29.5, 29.4, 24.9, 22.8, 14.7; IR (KBr) $\tilde{\nu}_{\max}$ = 3280–2423, 1710, 1670 cm⁻¹; elemental analysis calcd (%) for C₂₅H₃₅NO₃: C 75.53, H 8.87, N 3.52; found: C 75.62, H 8.76, N 3.54.

Spectroscopic measurements: Absorption spectra were recorded on a Hewlett–Packard 8453 diode array spectrophotometer, and the excitation and fluorescence spectra were obtained with Aminco-Bowman series 2 luminescence spectrometer. The fluorescence quantum yield was determined by using Coumarin 307 as a reference by the literature method.^[23]

Time resolved fluorescence (TRF): The time-correlated single-photon counting (TCSPC) method was used to record picosecond TRF. Output of a home-built cavity-dumped Kerr lens mode-locked Ti:sapphire laser running at 760 nm was doubled to generate excitation pulses at 380 nm. Fluorescence at the magic angle was detected by a thermoelectrically cooled MCP-PMT (Hamamatsu, R3809U-51). Instrument response function has a width of 40 ps full

width at half maximum to provide 8 ps time resolution with deconvolution.

Water solubility: The water solubility was determined by adding small increments of the dye solution in DMSO to a cuvette containing 3.0 mL of H₂O. In all cases, the DMSO content was maintained at 0.2%. The maximum concentration in the linear region in the plot of fluorescence intensity against the dye concentration was taken as the solubility (Figure S3).

pK_a value: The pK_a value of C-laurdan was estimated from the fluorescence titration curve as described by Cui et al.^[24]

Measurement of two-photon cross sections: The two-photon cross section δ was determined by using femtosecond fluorescence measurement technique as described by Pond and Lee.^[16,17] Samples were dissolved in EtOH (or H₂O) at concentrations of 3.0 μ M and the two-photon-induced fluorescence intensity was measured at 740–900 nm by using fluorescein (8.0 $\times 10^{-6}$ M, pH 11) as the reference, whose two-photon properties have been well characterized in the literature.^[18]

Vesicle preparation: Vesicles for the measurements of one-photon excitation and fluorescence spectra were prepared by the solvent evaporation method.^[25] The electroformation method was employed to grow GUVs.^[14,26,27] An imaging chamber (designed for field stimulation, RC-21BRFS, Warner Instruments Co.) modified for vesicle preparation (two parallel platinum electrodes separated between their surfaces 1 mm) was employed for this experiment. The temperature was measured inside the chamber at the platinum wires by using a digital thermometer with a precision of 0.1 °C. The probe in DMSO was added to the sample chamber after the vesicles were formed. The probe ratio in the vesicle was kept at greater than 300:1.

Cells: A431 cells were cultured in Dulbecco's modified Eagle's medium supplemented with penicillin/streptomycin and 10% fetal bovine serum in a CO₂ incubator at 37 °C. To test the colocalization of ganglioside G_{M1}, and high GP image of C-laurdan (or laurdan), A431 cells were treated with 150 nM BODIPY-G_{M1} (Molecular Probe) and 2.5 μ M C-laurdan (or laurdan) for 40 min at 4 °C, fixed with 3.7% formaldehyde, and observed in a spectral confocal multiphoton microscope.

One- and two-photon fluorescence microscopy: One- and two-photon fluorescence images were obtained with spectral confocal multiphoton microscopes (Leica TCS SP2) with a $\times 100$ oil-immersion objective, numerical aperture (NA)=1.30. For one-photon fluorescence microscopy, Ar-laser (488 nm excitation, 500–520 nm emission for BODIPY-G_{M1}) was used as the excitation source. Two-photon fluorescence microscopy images of the laurdan- and C-laurdan-labeled GUVs and cells were obtained by exciting the probes with a mode-locked titanium-sapphire laser (780 nm, Coherent Chameleon, 90 MHz, 200 fs). To obtain images at various wavelengths, internal PMTs were used to collect the signals in an 8 bit unsigned 1024 \times 1024 pixels at 400 Hz scan speed. The intensity images of laurdan and C-laurdan were recorded with the emission in the range of 400–460 nm and 470–530 nm with two channels of PMTs. The relative sensitivities of the two channels were determined for each experiment by using 0.5 μ M C-laurdan (or laurdan) in DMSO, and the G-factor in Equation (1) was calculated. For GP function images, a quarter wave-plate was aligned and placed before the microscope to minimize the polarization effects of the excitation light.

GP image: To quantify the emission spectral changes in the giant unilamellar vesicles (GUVs), the generalized polarization (GP) values

in Equation (1) have been calculated for each pixel by measuring the fluorescence intensities at 400–460 nm and 470–530 nm.^[13]

$$GP = \frac{I_{(400-460)} - G \times I_{(470-530)}}{I_{(400-460)} + G \times I_{(470-530)}} \quad (1)$$

Here, G is the sensitivity correction factor for the two different wavelength ranges. Background values, defined as less than 7% of the maximum intensity were set to zero and colored black (float type). GP distributions were obtained from the histograms of the GP values of the images and fitted to one or two Gaussian functions by the nonlinear fitting algorithm (Origin 7.0).

Acknowledgements

This work was supported by KOSEF (2006-03792) and CRM-KOSEF. H.J.C. and S.Y.J. were supported by the BK21 program. Y.G.K. was partially supported by IRC-KOSEF. T.J. acknowledges the support by the POSTECH core research area program.

Keywords: C-laurdan • fluorescent probes • lipid rafts • membranes • two-photon microscopy • vesicles

- [1] S. Munro, *Cell* **2003**, *115*, 377–388.
- [2] R. G. Anderson, *Annu. Rev. Biochem.* **1998**, *67*, 199–225.
- [3] M. Dykstra, A. Cherukuri, H. W. Sohn, S. J. Tzeng, S. K. Pierce, *Annu. Rev. Immunol.* **2003**, *21*, 457–481.
- [4] F. Galbiati, B. Razani, M. P. Lisanti, *Cell* **2001**, *106*, 403–411.
- [5] K. Simons, D. Toomre, *Nat. Rev. Mol. Cell Biol.* **2000**, *1*, 31–39.
- [6] E. O. Potma, X. S. Xie, *ChemPhysChem* **2005**, *6*, 77–79.
- [7] N. Kahya, D. Scherfeld, K. Bacia, B. Poolman, P. Schwille, *J. Biol. Chem.* **2003**, *278*, 28 109–28 115.
- [8] D. A. Zacharias, J. D. Violin, A. C. Newton, R. Y. Tsien, *Science* **2002**, *296*, 913–916.
- [9] J. C. Lawrence, D. E. Saslowsky, J. M. Edwardson, R. M. Henderson, *Biophys. J.* **2003**, *84*, 1827–1832.
- [10] C. Yuan, J. Furlong, P. Burgos, L. J. Johnston, *Biophys. J.* **2002**, *82*, 2526–2535.
- [11] W. H. Binder, V. Barragan, F. M. Menger, *Angew. Chem.* **2003**, *115*, 5980–6007; *Angew. Chem. Int. Ed.* **2003**, *42*, 5802–5827.
- [12] S. A. Sanchez, E. Gratton, *Acc. Chem. Res.* **2005**, *38*, 469–477.
- [13] K. Gaus, E. Gratton, E. P. Kable, A. S. Jones, I. Gelissen, L. Kritharides, W. Jessup, *Proc. Natl. Acad. Sci. USA* **2003**, *100*, 15 554–15 559.
- [14] L. A. Bagatolli, E. Gratton, *Biophys. J.* **1999**, *77*, 2090–2101.
- [15] T. Parasassi, E. Krasnowska, L. A. Bagatolli, E. Gratton, *J. Fluoresc.* **1998**, *8*, 365–373.
- [16] S. J. K. Pond, M. Rumi, M. D. Levin, T. C. Parker, D. Beljonne, M. W. Day, J.-L. Bredas, S. R. Marder, J. W. Perry, *J. Phys. Chem. A* **2002**, *106*, 11 470–11 480.
- [17] S. K. Lee, W. J. Yang, J. J. Choi, C. H. Kim, S. J. Jeon, B. R. Cho, *Org. Lett.* **2005**, *7*, 323–326.
- [18] C. Xu, W. W. Webb, *J. Opt. Soc. Am. B.* **1996**, *13*, 481–491.
- [19] L. A. Bagatolli, E. Gratton, *Biophys. J.* **2000**, *78*, 290–305.
- [20] P. W. Janes, S. C. Ley, A. I. Magee, *J. Cell Biol.* **1999**, *147*, 447–461.
- [21] B. W. Kim, H. J. Choo, J. W. Lee, J. H. Kim, Y. G. Ko, *Exp. Mol. Med.* **2004**, *36*, 476–485.
- [22] A. D. Douglass, R. D. Vale, *Cell* **2005**, *121*, 937–950.
- [23] J. N. Demas, G. A. Crosby, *J. Phys. Chem.* **1971**, *75*, 991–1024.
- [24] D. Cui, X. Qian, F. Liu, R. Zhang, *Org. Lett.* **2004**, *6*, 2757–2760.
- [25] A. Moscho, O. Orwar, D. T. Chiu, B. P. Modi, R. N. Zare, *Proc. Natl. Acad. Sci. USA* **1996**, *93*, 11 443–11 447.
- [26] M. I. Angelova, D. S. Dimitrov, *Faraday Discuss.* **1986**, *81*, 303–311.
- [27] F. M. Menger, M. I. Angelova, *Acc. Chem. Res.* **1998**, *31*, 789–797.

Received: January 3, 2007

Published online on February 15, 2007